



**HAL**  
open science

# Accurate Prediction of Adiabatic Ionization Energies for PAHs and Substituted Analogues

Jérémy Bourgalais, Xavier Mercier, Muneerah Mogren Al-Mogren, Majdi Hochlaf

► **To cite this version:**

Jérémy Bourgalais, Xavier Mercier, Muneerah Mogren Al-Mogren, Majdi Hochlaf. Accurate Prediction of Adiabatic Ionization Energies for PAHs and Substituted Analogues. *Journal of Physical Chemistry A*, 2023, 127 (40), pp.8447-8458. 10.1021/acs.jpca.3c04088 . hal-04234691

**HAL Id: hal-04234691**

**<https://hal.science/hal-04234691>**

Submitted on 10 Oct 2023

**HAL** is a multi-disciplinary open access archive for the deposit and dissemination of scientific research documents, whether they are published or not. The documents may come from teaching and research institutions in France or abroad, or from public or private research centers.

L'archive ouverte pluridisciplinaire **HAL**, est destinée au dépôt et à la diffusion de documents scientifiques de niveau recherche, publiés ou non, émanant des établissements d'enseignement et de recherche français ou étrangers, des laboratoires publics ou privés.

1 Accurate Prediction of Adiabatic Ionization Energies for  
2 PAHs and Substituted Analogues:  
3 *Advancements with the M06-2X Density Functional*  
4 *Theory Method*

5 Jérémy Bourgalais,<sup>1,\*</sup> Xavier Mercier,<sup>2</sup> Muneerah Mogren Al-Mogren,<sup>3</sup> and Majdi Hochlaf<sup>4,\*</sup>

6  
7  
8  
9  
10  
11  
12  
13  
14  
15  
16

17 **ABSTRACT**

18         Accurate calculation of AIEs for PAHs and their substituted analogues is important for  
19 understanding their electronic properties, reactivity, stability, and environmental/health  
20 implications. This work demonstrates that the M06-2X density functional theory (DFT) method  
21 performs well in predicting the adiabatic ionization energies (AIEs) of polycyclic aromatic  
22 hydrocarbons (PAHs) and related molecules, outperforming common DFT methods and competing  
23 in accuracy to the highly accurate CCSD(T)-F12 method. The accuracy of M06-2X is attributed to its  
24 large quantity of Hartree-Fock (HF) exchange and its ability to describe diffuse wave functions,  
25 which may make it suitable for predicting electronic properties associated with Rydberg-like  
26 electronic states. This suggests that M06-2X, with an appropriate basis set, is a reliable and  
27 efficient method for studying the PAHs and related molecules in conjunction with experimental  
28 techniques. The set of molecules used in this work includes also PAHs with hetero-atoms that can  
29 be found in biofuels or nucleic acid bases, making it of great interest for photoionization  
30 experiments and mass spectrometry. Down the road, this method will help understanding the  
31 relationship of various PAHs to graphene, guiding material research or electronic applications, and  
32 validating theoretical calculation methods.

33

34

35 Polycyclic aromatic hydrocarbons (PAHs) are a type of organic compound composed of fused  
36 aromatic rings. In PAHs, all carbon atoms are  $sp^2$  hybridized, resulting in a highly stable and fully  
37 conjugated delocalized aromatic  $\pi$ -electron system, which allows for a planar structure, assuming  
38 there are no steric repulsions present. PAHs are produced during incomplete combustion of organic  
39 matter and can be found in various environmental sources such as air, food, water, and soil.<sup>1-3</sup> Due  
40 to their wide distribution and potential toxicity, PAHs and their formation mechanisms have been  
41 extensively investigated in fields such as atmospheric sciences,<sup>4,5</sup> astrochemistry,<sup>6-8</sup> combustion  
42 science,<sup>9-13</sup> and material sciences.<sup>14,15</sup>

43 The ionization energy is a fundamental electronic property that plays a pivotal role in comprehending  
44 the properties and behavior of PAHs, as well as other organic compounds and materials. Precise  
45 predictions of PAH ionization energies can yield valuable insights into their chemical reactivity, as  
46 these energies are directly correlated to molecular stability and reactivity. Knowledge of PAH  
47 ionization energies can guide the design of novel materials targeting desired electronic properties  
48 and aid in the interpretation of experimental data, such as spectroscopic measurements and  
49 chemical reactions involving PAHs. Moreover, the ionization energy is closely intertwined with the  
50 electronic structure of PAHs, as it reflects the distribution and energy levels of molecular orbitals, as  
51 well as the stability of charged species. Understanding the electronic structure of PAHs is crucial for  
52 predicting their optical properties, electronic transport properties, and environmental behavior.  
53 Accurate predictions of ionization energies serve as a foundation for elucidating the behavior of PAHs  
54 in various systems and applications, and facilitate the optimization of PAH-based materials for  
55 diverse technological and environmental purposes.

56 The ionization energy of PAHs can be investigated through a combination of experimental and  
57 theoretical approaches. Experimental methods such as photoionization mass spectrometry and  
58 photoelectron spectroscopy involve exposing molecules to soft photon sources, typically in the  
59 vacuum ultraviolet (VUV) range, which promotes electrons from the ground state of neutral species  
60 to higher-energy states of the ionized respective compounds. By analyzing the photon energy at  
61 which the first ionization event occurs and examining the resulting mass spectra for fragmentation  
62 patterns and relative abundances of the ionized fragments, the ionization energies, as well as the  
63 molecular structure and properties, can be estimated. Photoelectron spectra can also provide  
64 information about the kinetic energies of the ejected electrons, which can offer insights into the  
65 ionization energy and electronic structure of PAHs.<sup>16-21</sup>

66 Theoretical calculations using quantum chemistry methods also complement experimental  
67 measurements by providing estimates of the ionization energy of molecules. These methods involve  
68 solving the electronic Schrödinger equation for the molecule and obtaining the ionization energy  
69 from the energy difference between the neutral and ionized states. Historically, the “gold standard”

70 quantum method for determining ionization energies of monoconfigurational molecular systems has  
71 been the coupled cluster method with singles, doubles, and perturbative triples ((R)CCSD(T)) in  
72 conjunction with the aug-cc-pVTZ atomic basis set, which is known for its high accuracy and  
73 predictive potentialities.<sup>22,23</sup> However, (R)CCSD(T) has a computational cost that scales steeply with  
74 the size of the system as it involves calculating higher-order excitations and requires extensive  
75 memory and storage, making it impractical for studying large molecules such as PAHs. Instead,  
76 density functional theory (DFT)<sup>24,25</sup> is a popular alternative to coupled clusters methods due to its  
77 computational efficiency and relatively good accuracy for a wide range of systems. However, despite  
78 its widespread success, the use of approximate exchange-correlation functionals provide different  
79 levels of accuracy, depending on the specific system being studied and the properties of interest.<sup>24,26</sup>  
80 In DFT, the electron density is treated as the basic variable, and the electron-electron correlation  
81 effects are approximated through the exchange-correlation functional.

82 In recent years, advancements in DFT methods, such as hybrid functionals, have shown promise in  
83 improving the accuracy of ionization energy calculations. However, the choice of functional can  
84 significantly impact the accuracy of predictions, and it is important to carefully select an appropriate  
85 functional for a given molecular system (see for instance Semmeq et al.<sup>27</sup>). In particular, hybrid  
86 functionals combine local exchange-correlation functional of DFT with a fraction of the exact  
87 exchange energy calculated from Hartree-Fock (HF) theory. The amount of HF exchange used in  
88 hybrid functionals is analogous to the electronic correlation energy considered in CCSD(T) *ab initio*  
89 methods. Electron correlation effects can be significant in PAHs due to their large size and  
90 delocalized  $\pi$ -electron systems, leading to strong static and dynamic correlation effects to be  
91 accounted for. Among hybrid functionals, M06-2X<sup>28</sup> is known for its accuracy in predicting a wide  
92 range of molecular properties, including bond lengths, bond angles, reaction energies, and  
93 noncovalent interactions. For ionization energies, M06-2X has been identified as the most promising  
94 functional within the Minnesota family<sup>29</sup> and exhibiting strong competitiveness with other  
95 functionals.<sup>30</sup>

96 In this work, we present a significant breakthrough in computational chemistry by demonstrating  
97 that M06-2X DFT can accurately calculate the adiabatic ionization energies (AIEs) of PAHs and  
98 substituted analogues across a wide range of molecular systems, having masses from low molecular  
99 mass (<100 u) to relatively high atomic mass (400 u). This work also demonstrates that the  
100 performance of M06-2X is comparable, in this context, to the widely regarded high-level *ab initio*  
101 explicitly correlated method (R)CCSD(T)-F12, which is used as reference for quantum chemical  
102 calculations. Indeed, this approach in conjunction with a basis set of aug-ccp-V(X)Z quality allows  
103 predicting molecular properties as accurate as the standard coupled clusters approach extrapolated  
104 to the complete basis set (CBS) limit, whereas a strong reduction of computational cost (both CPU

105 time and disks occupancy) is observed.<sup>19,31,32</sup> At the end of this manuscript, by employing the M06-2X  
106 method, predictions of the AIEs of coronene-derivatives are given and compared to the referenced  
107 AIE of graphene.

108

109 **Table 1.** Experimental reference AIE of naphthalene compared to the calculated AIEs using DFT and  
110 coupled cluster approaches. For DFT computations, we described the atoms using the 6-311++G(d,p)  
111 basis set.

Methods	AIE (eV)
Exp.	8.144 <sup>33</sup>
<b>DFT</b>	
M06-2X	8.144
B3LYP	7.867
$\omega$ b97X-D	7.953
B3PW91	7.912
PBE0	7.893
B97-2	7.804
CAM-B3LYP	7.974
TPSSh	7.759
X3LYP	7.828
<b>Composite</b>	
CBS-QB3	8.173
G4	8.143
<b>Coupled-clusters</b>	
(R)CCSD(T)/CBS	8.137
(R)CCSD(T)-F12/aug-cc-pVDZ	8.121

112

113 Naphthalene (C<sub>10</sub>H<sub>8</sub>, m/z 128 a.u.) with its two fused benzene rings has first been chosen as a  
114 benchmark system for validating theoretical models due to its well-defined and accurately  
115 determined experimental AIE value. Indeed, the AIE of naphthalene was experimentally determined  
116 to be 8.144 ± 0.0009 eV using a two-color multiphoton ionization technique.<sup>33</sup> Table 1 compares the  
117 reference AIE value of naphthalene to calculated values with some of the commonly used hybrid DFT

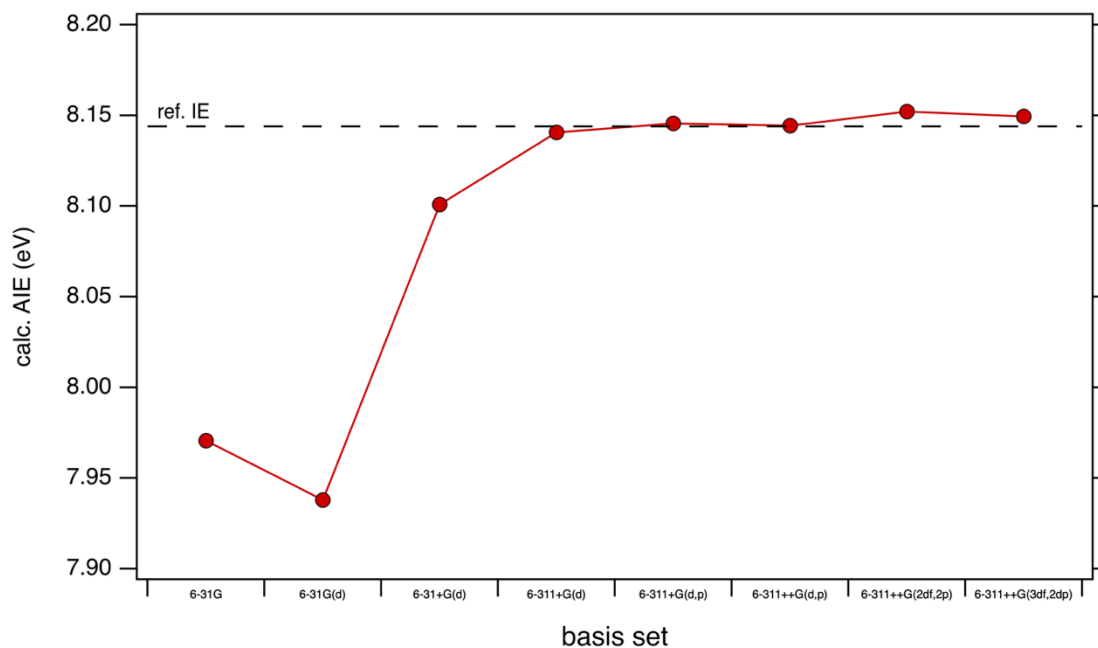
118 functionals in quantum chemistry and computational chemistry along with composite methods and  
119 coupled clusters calculations (see computational methods section for more details).

120 M06-2X in conjunction with the 6-311++G(d,p) Pople basis set<sup>34</sup> has by far the most accurate AIE  
121 value among the DFT methods with similar basis set size and is in an excellent agreement with the  
122 reference AIE value. M06-2X includes 54% of HF exchange, which is higher than the amount of HF  
123 exchange included in many other widely used hybrid DFT functionals, such as B3LYP<sup>35,36</sup> (20%), PBE0<sup>37</sup>  
124 (25%),  $\omega$ B97X-D<sup>38</sup> (10%). The higher amount of HF exchange in M06-2X can explain the present  
125 accurate determination compared to other DFT methods for naphthalene.

126 Interestingly, the AIE with M06-2X/6-311++G(d,p) is also more accurate than the values calculated  
127 with the composite methods (CBS-QB3, G4, Table 1). Typically, composite methods use a separate  
128 approach for geometry optimization and energy calculations. They employ high-level methods for  
129 energy calculations, while geometry optimization is performed using lower-level methods to reduce  
130 computational costs. The specific functional used for geometry optimization in composite methods  
131 may vary depending on the composite method being used. Some commonly used methods, such as  
132 the Gaussian-n (Gn) series of methods like G4<sup>39</sup>, employ HF or post-HF methods, such as MP2 or  
133 CCSD(T), for geometry optimizations. Other composite methods, such as the CBS-QB3<sup>40,41</sup> technique,  
134 use semiempirical methods, such as AM1 or PM3, for geometry optimizations. Semiempirical  
135 methods are approximate quantum mechanical methods that rely on simplified Hamiltonians and  
136 empirical parameters to describe molecular electronic structure. In G4, the geometry optimization is  
137 typically performed using a high-level *ab initio* method, that includes electron correlation effects  
138 beyond the mean-field approximation of the HF theory. This may explain the good agreement  
139 between G4 and M06-2X/6-311++G(d,p) for the AIE of naphthalene and the overestimation with CBS-  
140 QB3. Finally, the accuracy of M06-2X/6-311++G(d,p) is comparable to (R)CCSD(T) calculations for the  
141 AIE of naphthalene. The electronic structure based CBS extrapolation method typically involves using  
142 data from multiple levels of theory and basis sets to estimate the energy at the complete basis set  
143 limit, which is considered to be the most accurate result. In this case, if the CBS extrapolation was  
144 based on energies obtained from CCSD(T) calculations with cc-pVDZ and cc-pVTZ basis sets, there  
145 could be some limitations associated with the accuracy of these lower-level calculations. Besides,  
146 (R)CCSD(T)-F12 is a highly accurate post-SCF (self-consistent field) method that includes electron  
147 correlation effects explicitly. Table 1 shows that M06-2X/6-311++G(d,p) performs even better than  
148 this reference *ab initio* method. It is possible that for the AIE of naphthalene, the level of electron  
149 correlation included in M06-2X/6-311++G(d,p) is sufficient to provide accurate results, while the  
150 higher-order correlation effects captured by (R)CCSD(T)-F12/aug-cc-pVDZ may not be as crucial.

151 The choice of basis set can also impact the accuracy of calculated AIEs. (R)CCSD(T)-F12/aug-cc-pVDZ  
152 uses an augmented correlation-consistent basis set (in conjunction with the corresponding density

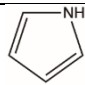
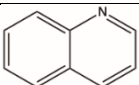
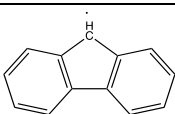
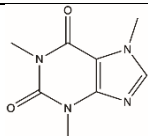
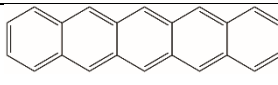
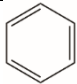
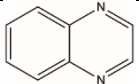
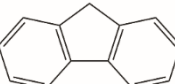
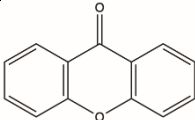
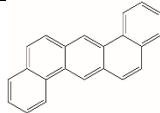
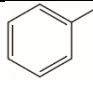
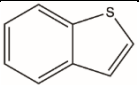
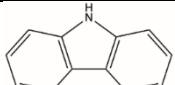
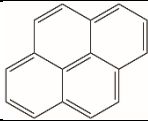

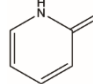
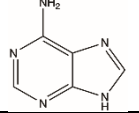
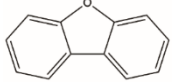
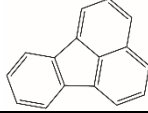
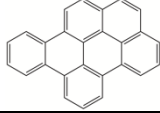
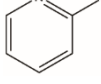
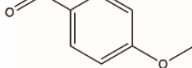
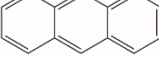
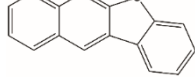

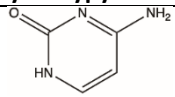
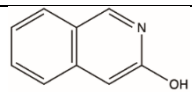
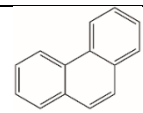
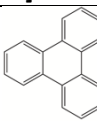
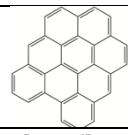
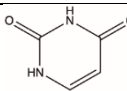
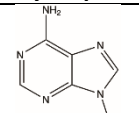
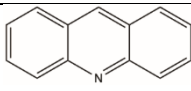
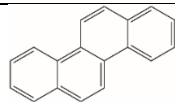
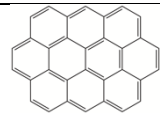
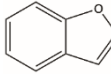
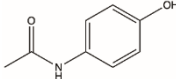
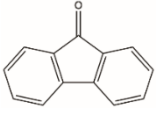
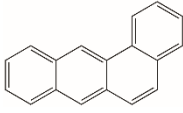
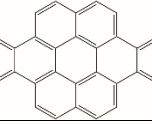
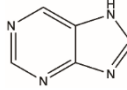
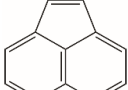
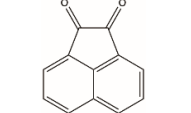
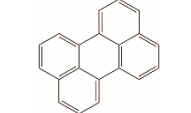
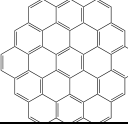
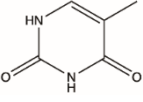
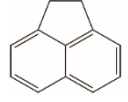
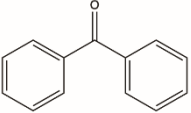
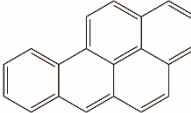
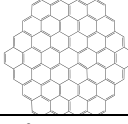
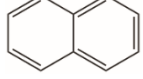
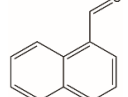
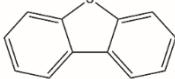

153 fitting and resolution of identity basis sets), while M06-2X/6-311++G(d,p) uses a DFT-specific basis  
154 set. The basis set size and quality can affect the description of electron orbitals and their energies,  
155 and can have an impact on the accuracy of calculated AIEs. Regarding the results, it seems that the  
156 basis set used in M06-2X/6-311++G(d,p) is better suited for describing the electronic structure of  
157 naphthalene in the context of AIE calculations.  
158



159 **Figure 1.** Calculated AIE of naphthalene using M06-2X with various Pople basis sets compared to the  
160 referenced ionization energy of naphthalene from Cockett et al.<sup>33</sup> (horizontal dashed line).  
161

162  
163 Basis set effects were probed to assess an appropriate level of theory for AIE calculations with the  
164 M06-2X functional and the 6-31G, 6-31G(d), 6-31+G(d), 6-311+G(d), 6-311+G(d,p), 6-311++G(d,p), 6-  
165 311++G(2df,2p), and 6-311++G(3df,2dp) basis sets. Figure 1 shows minimal changes in the AIE of  
166 naphthalene when different basis sets are used beyond M06-2X/6-311+G(d) and that the AIE is even  
167 overestimated when the basis set is increased to M06-2X/6-311++G(3df,2dp). One can think that the  
168 distribution of electron density near the ionization site may also be overestimated by basis sets with  
169 more diffuse functions. Diffuse functions are designed to capture electron density that is spread out  
170 over larger regions of space, including regions further away from the atomic nucleus. While they  
171 improve the accuracy of calculations involving long-range interactions and electron correlation, they  
172 may potentially lead to an overestimation of the AIE in certain cases. When the ionization process  
173 involves removing an electron from a localized orbital, the inclusion of diffuse functions can  
174 artificially enhance the electron density in the vicinity of the ionization site, resulting in an  
175 exaggerated stabilization effect.



				
<b>pyrrole</b>	<b>quinoline</b>	<b>fluorenyl</b>	<b>caffeine</b>	<b>pentacene</b>
				
<b>benzene</b>	<b>quinoxaline</b>	<b>fluorene</b>	<b>xanthone</b>	<b>dibenz[a,h]anthracene</b>
				
<b>toluene</b>	<b>benzo[b]thiophene</b>	<b>carbazole</b>	<b>pyrene</b>	<b>coronene</b>
				
<b>2-pyridone</b>	<b>adenine</b>	<b>dibenzofuran</b>	<b>fluoranthene</b>	<b>dibenzo[b,pqr]perylene</b>
				
<b>2-hydroxypyridine</b>	<b>anisaldehyde</b>	<b>anthracene</b>	<b>benzo[b]naphtho[2,3-d]furan</b>	<b>benzo[a]coronene</b>
				
<b>cytosine</b>	<b>3-hydroxyisoquinoline</b>	<b>phenanthrene</b>	<b>triphenylene</b>	<b>dibenzo[bc,ef]coronene</b>
				
<b>uracil</b>	<b>9-methyl adenine</b>	<b>acridine</b>	<b>chrysene</b>	<b>ovalene</b>
				
<b>2,3-benzofuran</b>	<b>paracetamol</b>	<b>fluorenone</b>	<b>benz[a]anthracene</b>	<b>dibenzo[a,j]coronene</b>
				
<b>purine</b>	<b>acenaphthylene</b>	<b>1,2-acenaphthenequinone</b>	<b>perylene</b>	<b>circumcoronene</b>
				
<b>thymine</b>	<b>acenaphthene</b>	<b>benzophenone</b>	<b>benzo[a]pyrene</b>	<b>circumcircumcoronene</b>
				

naphthalene	1-naphthaldehyde	dibenzothiophene	benzo[ghi]perylene
-------------	------------------	------------------	--------------------

178

179 **Table 3.** Calculated AIEs (in eV) in this work of various PAHs and substituted analogues with M06-  
180 2X/6-311+G(d), (R)CCSD(T)-F12/aug-cc-pVDZ and compared to reference experimental values from  
181 the literature. The chemical structures are given in Table 2. A hyphen indicates either the failure of  
182 convergence in the calculation or the absence of a reference for the AIE in the literature.

Molecular mass (u)	Name	Exp.	Calc. (M06-2X/6-311+G(d))	Calc. ((R)CCSD(T)-F12/aug-cc-pVDZ)
67	pyrrole	8.207 <sup>42</sup>	8.211	8.166
78	benzene	9.243 <sup>42</sup>	9.211	9.234
92	toluene	8.828 <sup>42</sup>	8.778	8.803
95	2-pyridone	8.443 <sup>43</sup>	8.482	8.430
	2-hydroxypyridine	8.933 <sup>43</sup>	8.942	8.916
111	cytosine	8.738 <sup>44</sup>	8.835	8.773
112	uracil	9.32 <sup>45</sup>	9.39	9.337
118	2,3-benzofuran	8.35 <sup>46</sup>	8.355	8.314
120	purine	9.12 <sup>45</sup>	9.33	9.122
126	thymine	8.913 <sup>47</sup>	8.931	8.909
128	naphthalene	8.144 <sup>42</sup>	8.141	8.121
129	quinoline	8.63 <sup>42</sup>	8.625	8.623
130	quinoxaline	8.89 <sup>48</sup>	9.015	8.882
134	Benzo[b]thiophene	8.73 <sup>42</sup>	8.758	-
136	anisaldehyde	8.60 <sup>42</sup>	8.611	8.542
135	adenine	8.264 <sup>49</sup>	8.294	8.260
145	3-hydroxyisoquinoline	8.028 <sup>50</sup>	8.08	8.065
149	9-methyl adenine	8.097 <sup>51</sup>	8.121	8.079
151	paracetamol	7.57	7.66	7.682
152	acenaphthylene	8.12 <sup>42</sup>	8.006	7.985
154	acenaphthene	7.75 <sup>42</sup>	7.695	7.682
156	1-naphthaldehyde	8.43 <sup>42</sup>	8.452	8.396
165	Fluorenyl	7.07 <sup>52</sup>	7.10	-
166	fluorene	7.91 <sup>42</sup>	7.918	7.881
167	carbazole	7.57 <sup>42</sup>	7.695	7.661
168	dibenzofuran	8.12 <sup>46</sup>	8.175	8.095
178	anthracene	7.439 <sup>42</sup>	7.388	7.400
	phenanthrene	7.89 <sup>42</sup>	7.898	7.891
179	acridine	7.8 <sup>42</sup>	7.896	7.888
180	fluorenone	8.356 <sup>53</sup>	8.406	8.491
182	1,2-acenaphthenequinone	8.77 <sup>42</sup>	8.867	8.776
	benzophenone	8.923 <sup>53</sup>	8.94	-
184	dibenzothiophene	7.90 <sup>42</sup>	7.993	-
194	caffeine	7.95 <sup>42</sup>	8.077	7.998
196	xanthone	8.42 <sup>42</sup>	8.508	8.440
202	pyrene	7.43 <sup>42</sup>	7.431	7.396
	fluoranthene	7.90 <sup>42</sup>	7.896	7.868
218	benzo[b]naphtho[2,3-	7.64 <sup>46</sup>	7.673	7.632

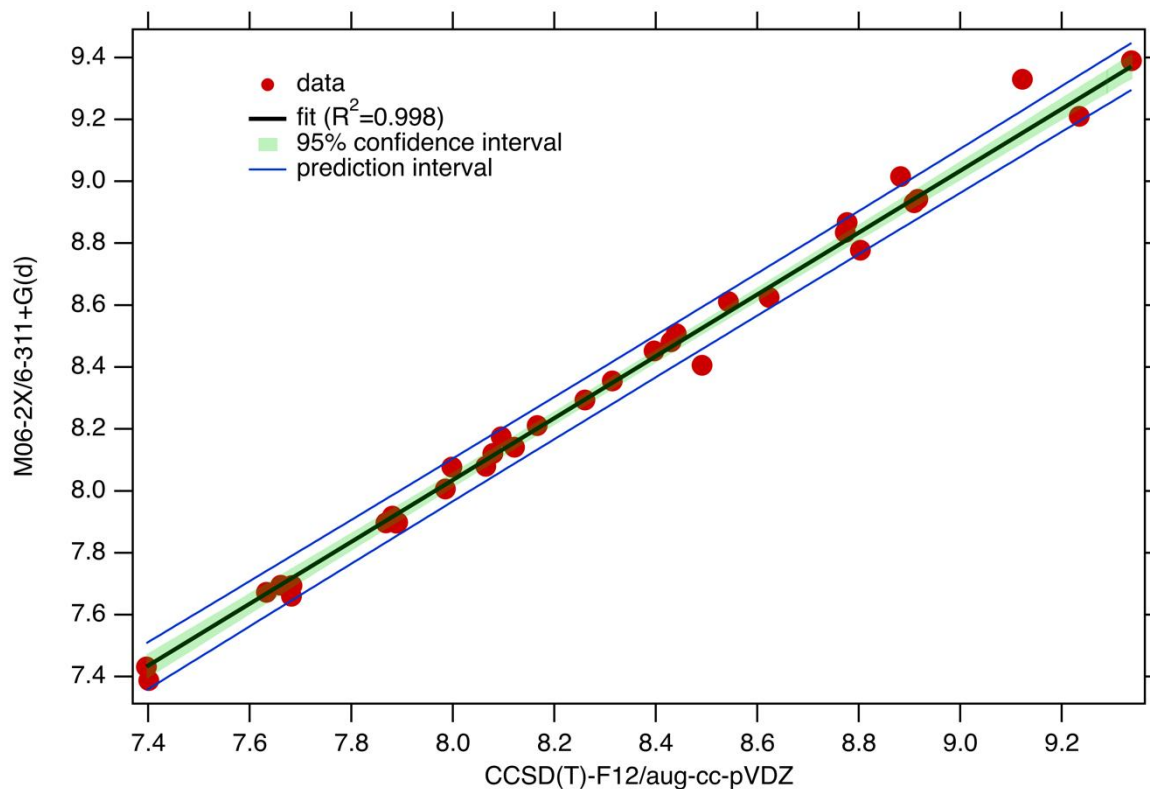
	d]furan			
228	triphenylene	7.87 <sup>42</sup>	7.892	-
	chrysene	7.60 <sup>42</sup>	7.585	-
	Benz[a]anthracene	7.45 <sup>42</sup>	7.391	-
252	perylene	6.96 <sup>42</sup>	6.965	-
	Benzo[a]pyrene	7.12 <sup>42</sup>	7.093	-
276	Benzo[ghi]perylene	7.17 <sup>42</sup>	7.171	-
278	pentacene	6.63 <sup>42</sup>	6.504	-
	Dibenz[a,h]anthracene	7.39 <sup>42</sup>	7.355	-
300	coronene	7.31 <sup>54</sup>	7.393	-
326	Dibenzo[b,pqr]perylene	7.12 <sup>42</sup>	7.206	-
350	Benzo[a]coronene	7.08 <sup>42</sup>	7.192	-
374	Dibenzo[bc,ef]coronene	6.50 <sup>42</sup>	6.521	-
398	ovalene	6.86 <sup>42</sup>	6.776	-
400	Dibenzo[a,j]coronene	6.92 <sup>42</sup>	7.007	-
666	circumcoronene	-	6.572	-
1,176	circumcircumcoronene	-	6.082	-

183

184

185 To verify the suitability of the M06-2X/6-311+G(d) method for calculating the AIEs of various PAHs  
186 and their substituted analogues, a specific investigation was conducted. Initially, the validity of this  
187 method was established by successfully calculating the AIE of naphthalene. Subsequently, in order to  
188 comprehensively explore the AIEs of a wide range of aromatic molecules, 54 PAHs and substituted  
189 analogues with masses ranging from 67 atomic mass unit (u) to 1,176 u (as detailed in Table 3) were  
190 subjected to AIE calculations using the M06-2X/6-311+G(d) method. These calculated AIE values  
191 were then compared to both the corresponding experimental values published in literature and the  
192 AIE values determined using the (R)CCSD(T)-F12/aug-cc-pVDZ method, which is considered as the  
193 reference method for AIE calculations.

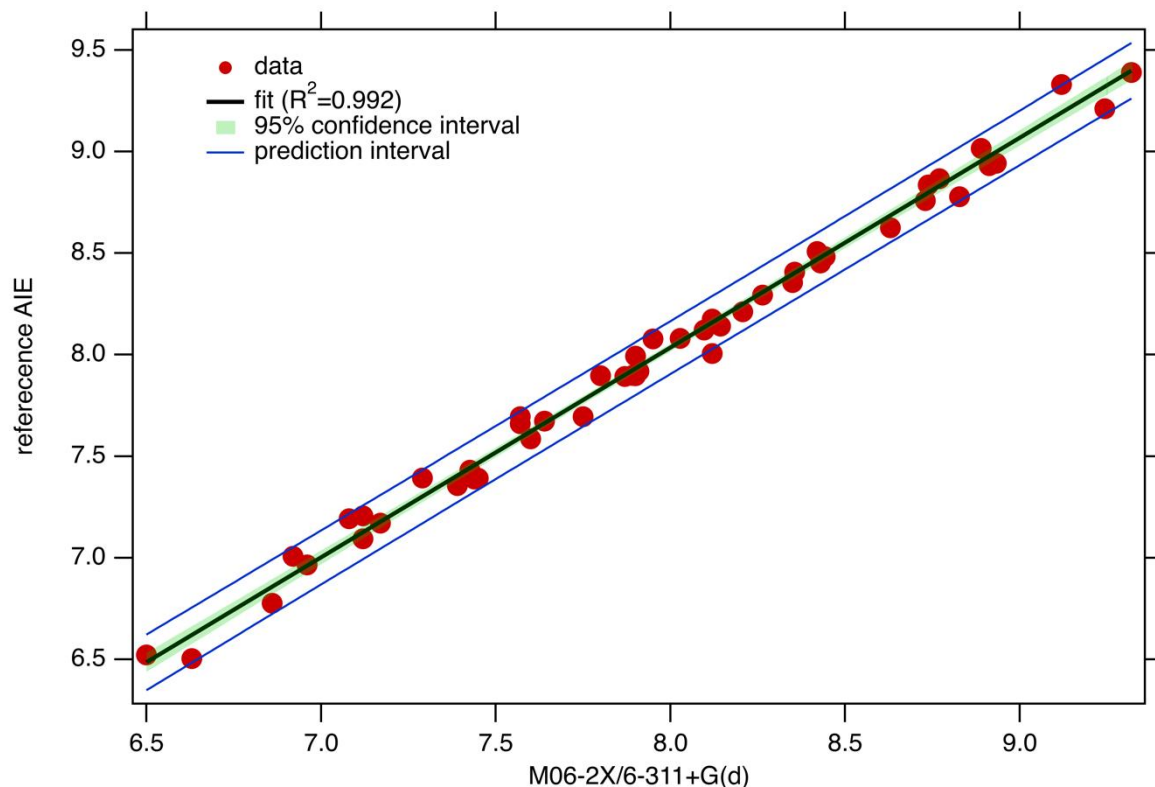
194



195  
 196 **Figure 2.** Plot of the calculated AIE for various PAHs and substituted analogues (as specified in Tables  
 197 2 and 3) with M06-2X/6-311+G(d) as a function of the AIE calculated with (R)CCSD(T)-F12/aug-cc-  
 198 pVDZ. The black line corresponds to the linear regression of the data. The green area shows a  
 199 confidence level to 95% and the blue line are prediction bands. The corresponding values are listed in  
 200 Table 3.

201  
 202 In Figure 2, a least-squares regression analysis is presented, showcasing the relationship between  
 203 the two sets of AIE values calculated using the M06-2X/6-311+G(d) and (R)CCSD(T)-F12/aug-cc-pVDZ  
 204 methods. Due to computational resource limitations, (R)CCSD(T)-F12 calculations were performed  
 205 for molecules with molar masses up to 218 u. The high correlation coefficient ( $R^2=0.998$ ) observed in  
 206 these data demonstrates a strong correlation, reinforcing the trend observed for naphthalene. This  
 207 finding indicates that the M06-2X/6-311+G(d) method is consistent and sufficiently reliable for  
 208 predicting the AIEs of these molecules.

209



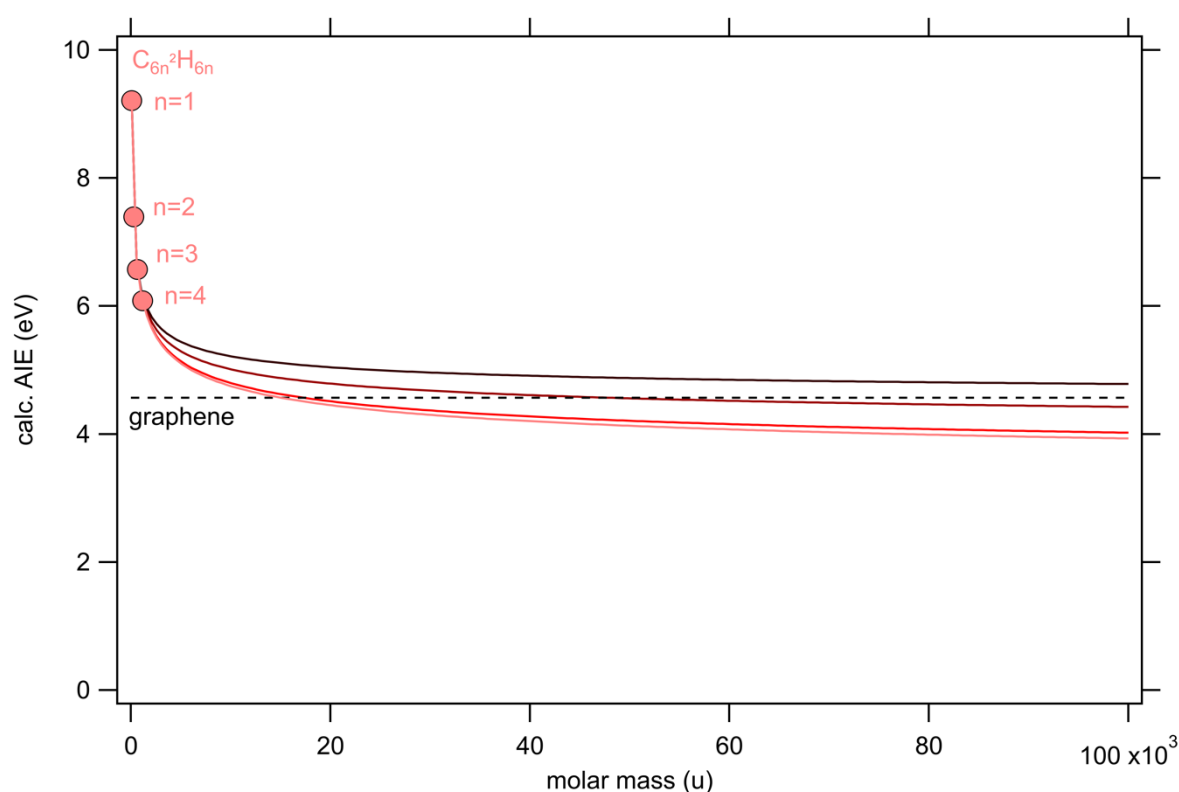
210  
 211 **Figure 3.** Comparison between calculated AIEs with M06-2X/6-311+G(d) and reference AIEs from the  
 212 literature for various PAHs and substituted analogues as specified in Tables 2 and 3.

213  
 214 To further expand the range of tested molecules and validate the reliability of the method, the  
 215 comparison between calculated AIEs using the M06-2X/6-311+G(d) method was extended to  
 216 experimental values reported in the literature. This included data from high-resolution photoelectron  
 217 photoion coincidence (PEPICO) spectroscopic studies (e.g., Laamiri et al.<sup>51</sup> and Schleier et al.<sup>48</sup>) as  
 218 well as information available in the National Institute of Standards and Technology (NIST) database.<sup>42</sup>  
 219 In this context, AIEs were calculated for 52 PAHs and substituted analogues, with molecular masses  
 220 ranging from 67 u to 400 u, using the M06-2X/6-311+G(d) computational method as listed in Table 2.  
 221 The molecular structures of these compounds consist of multiple fused benzene rings, with some  
 222 containing heteroatoms such as nitrogen (N), oxygen (O), sulfur (S), and various functional groups (as  
 223 detailed in Table 2). Figure 3 illustrates the least-squares regression analysis performed between the  
 224 experimental AIE values and the corresponding ones calculated using M06-2X/6-311+G(d). A high  
 225 correlation coefficient ( $R^2=0.992$ ) is obtained, indicating a strong correlation between the predicted  
 226 AIE values using M06-2X/6-311+G(d) and the reference values from the literature within the energy  
 227 range of 6.5 – 9.4 eV. Once again, this result provides further support for the remarkable reliability of  
 228 M06-2X/6-311+G(d) in predicting the AIEs of PAHs and substituted analogues, from relatively small  
 229 molecular systems to very large structures.

230 Tables 2 and 3 demonstrate that the predictive accuracy of the M06-2X/6-311+G(d) approach is  
231 valuable for distinguishing between structural isomers of PAHs, such as pyrene and fluoranthene  
232 ( $m/z$  202), which have a similar chemical formula ( $C_{16}H_{10}$ ) but differ in molecular structure. This  
233 structural distinction impacts the chemical and reactive properties of these compounds. The  
234 application of this theoretical method in investigating the formation of such isomers in  
235 photoionization experiments is highly significant for gaining insights into reaction  
236 mechanisms and exploring structure-property relationships.<sup>55</sup>

237 As shown in the case of fluorenyl ( $m/z$  165) and fluorene ( $m/z$  166), resonance-stabilized radicals are  
238 also one of the target of interest for this method with a high accuracy/time ratio. These radicals are  
239 expected to be involved in the formation of soot particles whose formation mechanisms remain  
240 incomplete.<sup>10</sup> The use of this theoretical method would thus benefit the photoionization experiments  
241 used for the characterization of large persistent radicals in nascent soot as well as obtaining  
242 structural information on the aromatic units.<sup>56</sup>

243



244  
245 **Figure 4.** Comparison between the calculated AIEs of  $C_{6n}^2H_{6n}$  ( $n = 1-4$ ) species (red dots) using the  
246 M06-2X/6-311+G(d) method and a reference value the ionization energy of graphene (black dashed  
247 line)<sup>57</sup>. Different fit of the data using a power function is represented by colored solid lines. Further  
248 information can be found in the text.

249

250 In order to provide predictive insights, AIE calculations were conducted using the benchmarked M06-  
251 2X/6-311+G(d) method for larger PAH systems that lack literature values. The focus was on  
252 investigating a specific group of coronene-derivative species with a general  $C_{6n^2}H_{6n}$  molecular  
253 formula. These compounds share a specific structural pattern characterized by the arrangement of  
254 six carbon atoms forming cyclic, aromatic configurations. In this work, the number of these cyclic  
255 units, denoted as  $n$ , was varied from 1 to 4 ( $C_6H_6$  to  $C_{96}H_{24}$ ), allowing for the exploration of a range of  
256 compounds from benzene to more complex structures: coronene, circumcoronene, and  
257 circumcircumcoronene. The AIEs obtained from calculations for coronene-derived species were  
258 compared to a referenced ionization potential of graphene:  $4.57 \pm 0.05$  eV.<sup>57</sup> The results, shown in  
259 Figure 4, indicate that as the size of the PAHs increases, their AIEs approach the value of graphene.  
260 This implies that the electrons become less tightly bound as the molecule size expands, indicating an  
261 evolution in the electronic structure of the PAHs. This observation aligns with the expectations  
262 derived from the Hückel simple model for such aromatic compounds. The fact that the ionization  
263 energies of PAHs approach that of graphene upon extending the  $\pi$ -aromatic system suggests a  
264 convergence of their electronic properties from molecules to extended 2D materials. This may  
265 indicate that large-sized PAHs exhibit electronic properties close to those of graphene, which can be  
266 important for potential applications such as the development of new PAH-based materials with  
267 interesting electrical conduction properties. The graphene-like electronic properties could also be  
268 useful in the design of electronic devices or in areas such as nanochemistry, nanotechnology,  
269 catalysis and energy conversion.

270 The AIEs of  $C_{6n^2}H_{6n}$  ( $n = 1-4$ ) species were fitted and extrapolated using a power function with the  
271 form  $y_0 + A x^B$ . In this equation, the constant term ( $y_0$ ) should correspond to the theoretical AIE of  
272 graphene. Figure 4 presents four fits using different values for the larger masses, resulting in  
273 significant variations in the  $y_0$  term and on the  $B$  power in this fitting function. This discrepancy  
274 arises because the calculated AIEs data primarily fall within the repulsive region of the fit rather than  
275 the convergent flat part. Accordingly, even when considering a PAH greater than 1,000 u, the AIE  
276 values remain considerably distant from that of graphene. Consequently, these species cannot be  
277 considered as substitutes for graphene in terms of their physico-chemical properties.

278 Furthermore, it is important to acknowledge that the differences between the reference value of  
279 graphene and the AIE values of PAHs could also be attributed to the presence of Jahn-Teller (JT)  
280 distortions in the cationic structures of PAHs. Similar to coronene, as discussed in Tampieri et al.<sup>58</sup>,  
281 both circumcoronene and circumcircumcoronene have highly symmetric neutral ground states with  
282 doubly degenerate HOMOs and LUMOs. When one electron is removed to form a cation, the partially  
283 filled degenerate molecular orbitals lead to an electronic instability. Consequently, this cation  
284 undergoes structural relaxation to minimize this instability. This relaxation manifests as a geometric

285 distortion, breaking the molecular symmetry and reducing the energy of the system. In this work, by  
286 considering the changes in bond length between the ionic and neutral forms, the relative elongation  
287 and restriction of the bond lengths are found to be consistent across different-sized PAHs but the  
288 overall extent of the changes diminishes as the molecules become larger.

289 To summarize this work shows that M06-2X outperforms the common DFT methods in predicting the  
290 AIEs of PAHs and substituted analogues. For those specific molecular systems, the level of accuracy  
291 of M06-2X is comparable to the highly accurate (R)CCSD(T)-F12 which is time consuming as the size  
292 of the molecular system increases. Comparison with existing AIE values from the literature shows  
293 that the M06-2X is also able to accurately predict the AIEs of large aromatic molecular systems. In  
294 this work the bigger structures whose AIE has been calculated includes 37 fused benzene rings and  
295 96 carbon atoms. Such accuracy from M06-2X is mainly related to the large quantity of HF exchange  
296 that this DFT contains compared to other DFTs. Another important aspect might also be the Rydberg  
297 character of certain excited states of PAHs which are highly excited electronic states with diffuse  
298 electron densities.<sup>59</sup> M06-2X has been designed to describe diffuse wave functions which could  
299 potentially make it suitable for accurately predicting properties associated with Rydberg-like states.<sup>60</sup>

300 This finding suggests that M06-2X, with the recommendation of a proper basis set, is a reliable and  
301 efficient method to be used in conjunction with experimental techniques for gaining a  
302 comprehensive understanding of the electronic properties of PAHs and related molecules.  
303 Particularly the low-lying Rydberg states, are not yet fully understood despite extensive research as  
304 the lowest members of the Rydberg series can deviate from pure Rydberg states due to the proximity  
305 to the molecular core. This results in mixing with valence states of similar energy, leading to complex  
306 electronic structures and spectroscopic features, are of considerable interest for combustion,  
307 atmospheric, molecular electronics<sup>61</sup> and astrochemistry<sup>62</sup>.

308 The set of molecules that was used to confront the predictions of M06-2X in this work includes PAHs  
309 with hetero-atoms that can be formed from biofuels or constitute nucleic acid bases. Thus having  
310 calculated AIEs to be able to identify those species in photoionization experiments using either  
311 coincidence detection schemes and mass spectrometry could be of great interest with many  
312 applications. Accurate calculation of AIEs for PAHs and their substituted analogues is important for  
313 understanding their electronic properties, predicting their reactivity and stability, designing  
314 functional materials, and evaluating their environmental and health implications. Since nucleobases  
315 (NBs) are the building blocks of both ribonucleic (RNA) and deoxyribonucleic acid (DNA), calculating  
316 the AIE of NBs is important for understanding the stability and reactivity of RNA and DNA, predicting  
317 DNA damage, studying DNA repair mechanisms, and aiding in drug design and development targeting  
318 nucleic acids. However, it is important to note that the accuracy and reliability of any computational  
319 method, including M06-2X, depend on the specific system being studied and the desired level of



320 accuracy. It is always prudent to validate the results of any computational method against  
321 experimental data or higher-level calculations to ensure the accuracy of the findings.

322

### 323 **COMPUTATIONAL METHODS**

324 All electronic structure and energy computations were performed using GAUSSIAN09<sup>63</sup> and  
325 MOLPRO<sup>64</sup> suites of *ab initio* programs. To compute AIEs, full structure optimizations on neutral and  
326 cationic species were carried out using tight convergence criteria and by formally lowering the  
327 symmetry in the calculations (i.e. in  $C_1$  point group). The optimized structure of the neutral species  
328 was used as the initial structure for the cationic forms. DFT and composite methods computations  
329 include full geometry optimizations and zero-point energy ( $\Delta ZPE$ ) correction. Coupled clusters  
330 methods, (R)CCSD(T)/CBS and (R)CCSD(T)-F12/aug-cc-pVDZ, as implemented in MOLPRO, were used  
331 for single point computations on top of the optimized neutral and cationic structures as determined  
332 by M06-2X/6-311+G(d). For the respective AIEs, we also used the  $\Delta ZPE$ , and frequencies as calculated  
333 at the M06-2X/6-311+G(d) level of theory. Only for the biggest species calculated in this work,  $C_{96}H_{24}$ ,  
334 the  $\Delta ZPE$  was derived from frequency calculations at the M06-2X/6-31G(d) level of theory after  
335 optimization. The CCSD(T)/CBS energies were extrapolated from CCSD(T)/cc-pVDZ, and CCSD(T)/cc-  
336 pVTZ energies using the scheme suggested by Martin<sup>65</sup> and Feller and Dixon<sup>66</sup>.

337

### 338 **AUTHOR INFORMATION**

339 Corresponding authors

340 **Jérémy Bourgalais** - Université de Lorraine, CNRS, LRGP, F-54000 Nancy, France ; ORCID : 0000-0003-  
341 4710-8943 ; Email : [jeremy.bourgalais@cnrs.fr](mailto:jeremy.bourgalais@cnrs.fr)

342 **Majdi Hochlaf** - Université Gustave Eiffel, COSYS/IMSE, 77454 Champs sur Marne, France ; ORCID :  
343 0000-0002-4737-7978 ; Email : [majdi.hochlaf@univ-eiffel.fr](mailto:majdi.hochlaf@univ-eiffel.fr)

344

### 345 **AUTHORS**

346 **Xavier Mercier**

347 Université de Lille, CNRS, PC2A, F-59000, Lille, France. Email: [xavier.mercier@univ-lille.fr](mailto:xavier.mercier@univ-lille.fr)

348 **Muneerah Mogren Al-Mogren**

349 Department of Chemistry, College of Sciences, King Saud University, PO Box 2455, Riyadh 11451,  
350 Saudi Arabia. Email: [mmogren@ksu.edu.sa](mailto:mmogren@ksu.edu.sa)

351

### 352 **ACKNOWLEDGEMENTS**

353 This work was performed using HPC resources from GENCI-IDRIS (Grant 2023-AD010814091) and the  
354 EXPLOR centre hosted by the University of Lorraine (Project: 2021EXTXX2356). The authors extend

355 their appreciation to the Researchers supporting project number (RSPD2023R808) King Saud  
356 University, Riyadh, Saudi Arabia. The authors thank Prof. C. Adamo (France) for engaging in fruitful  
357 discussions.  
358

- 360 (1) Idowu, O.; Semple, K. T.; Ramadass, K.; O'Connor, W.; Hansbro, P.; Thavamani, P.  
361 Beyond the Obvious: Environmental Health Implications of Polar Polycyclic Aromatic  
362 Hydrocarbons. *Environment International* **2019**, *123*, 543–557.  
363 <https://doi.org/10.1016/j.envint.2018.12.051>.
- 364 (2) Sampaio, G. R.; Guizzellini, G. M.; da Silva, S. A.; de Almeida, A. P.; Pinaffi-Langley,  
365 A. C. C.; Rogero, M. M.; de Camargo, A. C.; Torres, E. A. F. S. Polycyclic Aromatic  
366 Hydrocarbons in Foods: Biological Effects, Legislation, Occurrence, Analytical Methods, and  
367 Strategies to Reduce Their Formation. *International Journal of Molecular Sciences* **2021**, *22*  
368 (11), 6010. <https://doi.org/10.3390/ijms22116010>.
- 369 (3) Premnath, N.; Mohanrasu, K.; Guru Raj Rao, R.; Dinesh, G. H.; Prakash, G. S.;  
370 Ananthi, V.; Ponnuchamy, K.; Muthusamy, G.; Arun, A. A Crucial Review on Polycyclic  
371 Aromatic Hydrocarbons - Environmental Occurrence and Strategies for Microbial  
372 Degradation. *Chemosphere* **2021**, *280*, 130608.  
373 <https://doi.org/10.1016/j.chemosphere.2021.130608>.
- 374 (4) Keyte, I. J.; Harrison, R. M.; Lammel, G. Chemical Reactivity and Long-Range  
375 Transport Potential of Polycyclic Aromatic Hydrocarbons—a Review. *Chemical Society*  
376 *Reviews* **2013**, *42* (24), 9333–9391.
- 377 (5) Kim, K.-H.; Jahan, S. A.; Kabir, E.; Brown, R. J. A Review of Airborne Polycyclic  
378 Aromatic Hydrocarbons (PAHs) and Their Human Health Effects. *Environment international*  
379 **2013**, *60*, 71–80.
- 380 (6) Parker, D. S. N.; Kaiser, R. I. On the Formation of Nitrogen-Substituted Polycyclic  
381 Aromatic Hydrocarbons (NPAHs) in Circumstellar and Interstellar Environments. *Chem. Soc.*  
382 *Rev.* **2017**, *46* (2), 452–463. <https://doi.org/10.1039/C6CS00714G>.
- 383 (7) Kaiser, R. I.; Parker, D. S.; Mebel, A. M. Reaction Dynamics in Astrochemistry: Low-  
384 Temperature Pathways to Polycyclic Aromatic Hydrocarbons in the Interstellar Medium.  
385 *Annual Review of Physical Chemistry* **2015**, *66*, 43–67.
- 386 (8) Joblin, C.; Tielens, A. G. G. M. *PAHs and the Universe*; EDP Sciences, 2021.
- 387 (9) Richter, H.; Howard, J. B. Formation of Polycyclic Aromatic Hydrocarbons and Their  
388 Growth to Soot—a Review of Chemical Reaction Pathways. *Progress in Energy and*  
389 *Combustion science* **2000**, *26* (4–6), 565–608.
- 390 (10) Johansson, K. O.; Head-Gordon, M. P.; Schrader, P. E.; Wilson, K. R.; Michelsen, H.  
391 A. Resonance-Stabilized Hydrocarbon-Radical Chain Reactions May Explain Soot Inception  
392 and Growth. *Science* **2018**, *361* (6406), 997–1000. <https://doi.org/10.1126/science.aat3417>.
- 393 (11) Homann, K.-H. Fullerenes and Soot Formation—New Pathways to Large Particles in  
394 Flames. *Angewandte Chemie International Edition* **1998**, *37* (18), 2434–2451.
- 395 (12) Wang, H. Formation of Nascent Soot and Other Condensed-Phase Materials in  
396 Flames. *Proceedings of the Combustion institute* **2011**, *33* (1), 41–67.
- 397 (13) Frenklach, M. Reaction Mechanism of Soot Formation in Flames. *Physical chemistry*  
398 *chemical Physics* **2002**, *4* (11), 2028–2037.
- 399 (14) Anthony, J. E. Functionalized Acenes and Heteroacenes for Organic Electronics.  
400 *Chemical reviews* **2006**, *106* (12), 5028–5048.
- 401 (15) Anthony, J. E. The Larger Acenes: Versatile Organic Semiconductors. *Angewandte*  
402 *Chemie International Edition* **2008**, *47* (3), 452–483.
- 403 (16) Fischer, I.; Pratt, S. T. Photoelectron Spectroscopy in Molecular Physical Chemistry.  
404 *Phys. Chem. Chem. Phys.* **2022**, *24* (4), 1944–1959. <https://doi.org/10.1039/D1CP04984D>.
- 405 (17) Hemberger, P.; Bodi, A.; Bierkandt, T.; Köhler, M.; Kaczmarek, D.; Kasper, T.  
406 Photoelectron Photoion Coincidence Spectroscopy Provides Mechanistic Insights in Fuel  
407 Synthesis and Conversion. *Energy Fuels* **2021**, *35* (20), 16265–16302.  
408 <https://doi.org/10.1021/acs.energyfuels.1c01712>.

409 (18) Baer, T.; P. Tuckett, R. Advances in Threshold Photoelectron Spectroscopy (TPES)  
410 and Threshold Photoelectron Photoion Coincidence (TPEPICO). *Physical Chemistry*  
411 *Chemical Physics* **2017**, *19* (15), 9698–9723. <https://doi.org/10.1039/C7CP00144D>.  
412 (19) Hochlaf, M. Advances in Spectroscopy and Dynamics of Small and Medium Sized  
413 Molecules and Clusters. *Physical Chemistry Chemical Physics* **2017**, *19* (32), 21236–21261.  
414 <https://doi.org/10.1039/C7CP01980G>.  
415 (20) Dyke, J. M. Photoionization Studies of Reactive Intermediates Using Synchrotron  
416 Radiation. *Phys. Chem. Chem. Phys.* **2019**, *21* (18), 9106–9136.  
417 <https://doi.org/10.1039/C9CP00623K>.  
418 (21) Mercier, X.; Faccinetto, A.; Batut, S.; Vanhove, G.; Božanić, D. K.; Hróðmarsson, H.  
419 R.; Garcia, G. A.; Nahon, L. Selective Identification of Cyclopentaring-Fused PAHs and  
420 Side-Substituted PAHs in a Low Pressure Premixed Sooting Flame by Photoelectron  
421 Photoion Coincidence Spectroscopy. *Phys. Chem. Chem. Phys.* **2020**, *22* (28), 15926–15944.  
422 <https://doi.org/10.1039/D0CP02740E>.  
423 (22) Purvis III, G. D.; Bartlett, R. J. A Full Coupled-Cluster Singles and Doubles Model:  
424 The Inclusion of Disconnected Triples. *The Journal of Chemical Physics* **1982**, *76* (4), 1910–  
425 1918.  
426 (23) Raghavachari, K.; Trucks, G. W.; Pople, J. A.; Head-Gordon, M. A Fifth-Order  
427 Perturbation Comparison of Electron Correlation Theories. *Chemical Physics Letters* **1989**,  
428 *157* (6), 479–483.  
429 (24) Cohen, A. J.; Mori-Sánchez, P.; Yang, W. Challenges for Density Functional Theory.  
430 *Chemical reviews* **2012**, *112* (1), 289–320.  
431 (25) Friesner, R. A. Ab Initio Quantum Chemistry: Methodology and Applications.  
432 *Proceedings of the National Academy of Sciences* **2005**, *102* (19), 6648–6653.  
433 (26) Hammes-Schiffer, S. A Conundrum for Density Functional Theory. *Science* **2017**, *355*  
434 (6320), 28–29.  
435 (27) Semmeq, A.; Ouaskit, S.; Monari, A.; Badawi, M. Ionization and Fragmentation of  
436 Uracil upon Microhydration. *Phys. Chem. Chem. Phys.* **2019**, *21* (9), 4810–4821.  
437 <https://doi.org/10.1039/C8CP07452F>.  
438 (28) Zhao, Y.; Truhlar, D. G. The M06 Suite of Density Functionals for Main Group  
439 Thermochemistry, Thermochemical Kinetics, Noncovalent Interactions, Excited States, and  
440 Transition Elements: Two New Functionals and Systematic Testing of Four M06-Class  
441 Functionals and 12 Other Functionals. *Theor Chem Account* **2008**, *120* (1), 215–241.  
442 <https://doi.org/10.1007/s00214-007-0310-x>.  
443 (29) Mardirossian, N.; Head-Gordon, M. How Accurate Are the Minnesota Density  
444 Functionals for Noncovalent Interactions, Isomerization Energies, Thermochemistry, and  
445 Barrier Heights Involving Molecules Composed of Main-Group Elements? *J. Chem. Theory*  
446 *Comput.* **2016**, *12* (9), 4303–4325. <https://doi.org/10.1021/acs.jctc.6b00637>.  
447 (30) Goerigk, L.; Hansen, A.; Bauer, C.; Ehrlich, S.; Najibi, A.; Grimme, S. A Look at the  
448 Density Functional Theory Zoo with the Advanced GMTKN55 Database for General Main  
449 Group Thermochemistry, Kinetics and Noncovalent Interactions. *Physical Chemistry*  
450 *Chemical Physics* **2017**, *19* (48), 32184–32215.  
451 (31) Zhang, J.; Valeev, E. F. Prediction of Reaction Barriers and Thermochemical  
452 Properties with Explicitly Correlated Coupled-Cluster Methods: A Basis Set Assessment.  
453 *Journal of chemical theory and computation* **2012**, *8* (9), 3175–3186.  
454 (32) Tew, D. P. Principal Domains in F12 Explicitly Correlated Theory. In *Advances in*  
455 *Quantum Chemistry*; Elsevier, 2021; Vol. 83, pp 83–106.  
456 (33) Cockett, M. C.; Ozeki, H.; Okuyama, K.; Kimura, K. Vibronic Coupling in the  
457 Ground Cationic State of Naphthalene: A Laser Threshold Photoelectron [Zero Kinetic  
458 Energy (ZEKE)-Photoelectron] Spectroscopic Study. *The Journal of chemical physics* **1993**,

459 98 (10), 7763–7772.  
460 (34) Ditchfield, R.; Hehre, W. J.; Pople, J. A. Self- Consistent Molecular- Orbital  
461 Methods. IX. An Extended Gaussian- Type Basis for Molecular- Orbital Studies of Organic  
462 Molecules. *J. Chem. Phys.* **1971**, *54* (2), 724–728. <https://doi.org/10.1063/1.1674902>.  
463 (35) Becke, A. D. A New Mixing of Hartree–Fock and Local Density-Functional Theories.  
464 *The Journal of chemical physics* **1993**, *98* (2), 1372–1377.  
465 (36) Stephens, P. J.; Devlin, F. J.; Chabalowski, C. F.; Frisch, M. J. Ab Initio Calculation  
466 of Vibrational Absorption and Circular Dichroism Spectra Using Density Functional Force  
467 Fields. *The Journal of physical chemistry* **1994**, *98* (45), 11623–11627.  
468 (37) Adamo, C.; Barone, V. Toward Reliable Density Functional Methods without  
469 Adjustable Parameters: The PBE0 Model. *J. Chem. Phys.* **1999**, *110* (13), 6158–6170.  
470 <https://doi.org/10.1063/1.478522>.  
471 (38) Chai, J.-D.; Head-Gordon, M. Systematic Optimization of Long-Range Corrected  
472 Hybrid Density Functionals. *The Journal of Chemical Physics* **2008**, *128* (8), 084106.  
473 <https://doi.org/10.1063/1.2834918>.  
474 (39) Curtiss, L. A.; Redfern, P. C.; Raghavachari, K. Gaussian-4 Theory. *J. Chem. Phys.*  
475 **2007**, *126* (8), 084108. <https://doi.org/10.1063/1.2436888>.  
476 (40) Montgomery, J. A.; Frisch, M. J.; Ochterski, J. W.; Petersson, G. A. A Complete Basis  
477 Set Model Chemistry. VI. Use of Density Functional Geometries and Frequencies. *J. Chem.*  
478 *Phys.* **1999**, *110* (6), 2822–2827. <https://doi.org/10.1063/1.477924>.  
479 (41) Montgomery, J. A.; Frisch, M. J.; Ochterski, J. W.; Petersson, G. A. A Complete Basis  
480 Set Model Chemistry. VII. Use of the Minimum Population Localization Method. *J. Chem.*  
481 *Phys.* **2000**, *112* (15), 6532–6542. <https://doi.org/10.1063/1.481224>.  
482 (42) Linstrom, P. J.; Mallard, W. G.; Eds. *NIST Chemistry WebBook, NIST Standard*  
483 *Reference Database Number 69*. National Institute of Standards and Technology,  
484 Gaithersburg MD, 20899 (accessed 2023-01-10).  
485 (43) Pouilly, J. C.; Schermann, J. P.; Nieuwjaer, N.; Lecomte, F.; Grégoire, G.; Desfrancois,  
486 C.; Garcia, G. A.; Nahon, L.; Nandi, D.; Poisson, L.; Hochlaf, M. Photoionization of 2-  
487 Pyridone and 2-Hydroxypyridine. *Phys. Chem. Chem. Phys.* **2010**, *12* (14), 3566.  
488 <https://doi.org/10.1039/b923630a>.  
489 (44) chen, Z.; Lau, K.-C.; Garcia, G. A.; Nahon, L.; Bozanic, D. K.; Poisson, L.; Al-  
490 Mogren, M. M.; Schwell, M.; Francisco, J. S.; Bellili, A.; Hochlaf, M. Identifying Cytosine-  
491 Specific Isomers via High-Accuracy Single Photon Ionization | Journal of the American  
492 Chemical Society. *Journal of the American Chemical Society* **2016**, *138* (51), 16596–16599.  
493 <https://doi.org/10.1021/jacs.6b10413>.  
494 (45) Orlov, V. M.; Smirnov, A. N.; Varshavsky, Y. M. Ionization Potentials and Electron-  
495 Donor Ability of Nucleic Acid Bases and Their Analogues. *Tetrahedron Letters* **1976**, *48*,  
496 4377.  
497 (46) Mayer, P. M.; Bodi, A. VUV Photoprocessing of Oxygen-Containing Polycyclic  
498 Aromatic Hydrocarbons: Threshold Photoelectron Spectra. *Journal of Molecular*  
499 *Spectroscopy* **2021**, *377*, 111446. <https://doi.org/10.1016/j.jms.2021.111446>.  
500 (47) Majdi, Y.; Hochlaf, M.; Pan, Y.; Lau, K.-C.; Poisson, L.; Garcia, G. A.; Nahon, L.;  
501 Al-Mogren, M. M.; Schwell, M. Theoretical and Experimental Photoelectron Spectroscopy  
502 Characterization of the Ground State of Thymine Cation. *J. Phys. Chem. A* **2015**, *119* (23),  
503 5951–5958. <https://doi.org/10.1021/jp510716c>.  
504 (48) Schleier, D.; Hemberger, P.; Bodi, A.; Bouwman, J. Threshold Photoelectron  
505 Spectroscopy of Quinoxaline, Quinazoline, and Cinnoline. *J. Phys. Chem. A* **2022**, *126* (14),  
506 2211–2221. <https://doi.org/10.1021/acs.jpca.2c01073>.  
507 (49) Zhao, H. Y.; Lau, K.-C.; Garcia, G. A.; Nahon, L.; Carniato, S.; Poisson, L.; Schwell,  
508 M.; Al-Mogren, M. M.; Hochlaf, M. Unveiling the Complex Vibronic Structure of the

509 Canonical Adenine Cation. *Physical Chemistry Chemical Physics* **2018**, *20* (32), 20756–  
510 20765.

511 (50) Pan, Y.; Lau, K.-C.; Poisson, L.; Garcia, G. A.; Nahon, L.; Hochlaf, M. Slow  
512 Photoelectron Spectroscopy of 3-Hydroxyisoquinoline. *The Journal of Physical Chemistry A*  
513 **2013**, *117*, 8095–8102. <https://doi.org/10.1021/jp311615u>.

514 (51) Laamiri, K.; A. Garcia, G.; Nahon, L.; Houria, A. B.; Feifel, R.; Hochlaf, M.  
515 Threshold Photoelectron Spectroscopy of 9-Methyladenine: Theory and Experiment. *Physical*  
516 *Chemistry Chemical Physics* **2022**, *24*, 3523–3531. <https://doi.org/10.1039/D1CP03729C>.

517 (52) Lang, M.; Holzmeier, F.; Fischer, I.; Hemberger, P. Threshold Photoionization of  
518 Fluorenyl, Benzhydryl, Diphenylmethylene, and Their Dimers. *J. Phys. Chem. A* **2013**, *117*  
519 (25), 5260–5268. <https://doi.org/10.1021/jp403158z>.

520 (53) Goud, Z.; Röder, A.; Miranda, B. K. C. de; Gaveau, M.-A.; Briant, M.; Soep, B.;  
521 Mestdagh, J.-M.; Hochlaf, M.; Poisson, L. Energetics and Ionization Dynamics of Two  
522 Diarylketone Molecules: Benzophenone and Fluorenone. *Physical Chemistry Chemical*  
523 *Physics* **2019**, *21* (26), 14453–14464. <https://doi.org/10.1039/C9CP02385B>.

524 (54) Clar, E.; Schmidt, W. Correlations between Photoelectron and Ultraviolet Absorption  
525 Spectra of Polycyclic Hydrocarbons. The Perylene, Coronene and Bisanthene Series.  
526 *Tetrahedron* **1977**, *33* (16), 2093–2097.

527 (55) Sinha, S.; Rahman, R. K.; Raj, A. On the Role of Resonantly Stabilized Radicals in  
528 Polycyclic Aromatic Hydrocarbon (PAH) Formation: Pyrene and Fluoranthene Formation  
529 from Benzyl–Indenyl Addition. *Phys. Chem. Chem. Phys.* **2017**, *19* (29), 19262–19278.  
530 <https://doi.org/10.1039/C7CP02539D>.

531 (56) Faccinetto, A.; Irimiea, C.; Minutolo, P.; Commodo, M.; D’Anna, A.; Nuns, N.;  
532 Carpentier, Y.; Pirim, C.; Desgroux, P.; Focsa, C.; Mercier, X. Evidence on the Formation of  
533 Dimers of Polycyclic Aromatic Hydrocarbons in a Laminar Diffusion Flame. *Commun Chem*  
534 **2020**, *3* (1), 112. <https://doi.org/10.1038/s42004-020-00357-2>.

535 (57) Yu, Y.-J.; Zhao, Y.; Ryu, S.; Brus, L. E.; Kim, K. S.; Kim, P. Tuning the Graphene  
536 Work Function by Electric Field Effect. *Nano Lett.* **2009**, *9* (10), 3430–3434.  
537 <https://doi.org/10.1021/nl901572a>.

538 (58) Tampieri, F.; Barbon, A.; Tommasini, M. Analysis of the Jahn-Teller Effect in  
539 Coronene and Corannulene Ions and Its Effect in EPR Spectroscopy. *Chemical Physics*  
540 *Impact* **2021**, *2*, 100012. <https://doi.org/10.1016/j.chphi.2021.100012>.

541 (59) Robin, M. B. *Higher Excited States of Polyatomic Molecules*; Academic Press: New  
542 York, 1974.

543 (60) Jacquemin, D.; Perpète, E. A.; Ciofini, I.; Adamo, C.; Valero, R.; Zhao, Y.; Truhlar,  
544 D. G. On the Performances of the M06 Family of Density Functionals for Electronic  
545 Excitation Energies. *Journal of Chemical Theory and Computation* **2010**, *6* (7), 2071–2085.

546 (61) Feng, X.; Pisula, W.; Müllen, K. Large Polycyclic Aromatic Hydrocarbons: Synthesis  
547 and Discotic Organization. *Pure and Applied Chemistry* **2009**, *81* (12), 2203–2224.  
548 <https://doi.org/10.1351/PAC-CON-09-07-07>.

549 (62) Tielens, A. G. G. M. Interstellar Polycyclic Aromatic Hydrocarbon Molecules. *Annu.*  
550 *Rev. Astron. Astrophys.* **2008**, *46* (1), 289–337.  
551 <https://doi.org/10.1146/annurev.astro.46.060407.145211>.

552 (63) Frisch, M. J.; Trucks, G. W.; Schlegel, H. B.; Scuseria, G. E.; Robb, M. A.;  
553 Cheeseman, J. R.; Scalmani, G.; Barone, V.; Petersson, G. A.; Nakatsuji, H.; Li, X.; Caricato,  
554 M.; Marenich, A. V.; Bloino, J.; Janesko, B. G.; Gomperts, R.; Mennucci, B.; Hratchian, H.  
555 P.; Ortiz, J. V.; Izmaylov, A. F.; Sonnenberg, J. L.; Williams; Ding, F.; Lipparini, F.; Egidi,  
556 F.; Goings, J.; Peng, B.; Petrone, A.; Henderson, T.; Ranasinghe, D.; Zakrzewski, V. G.; Gao,  
557 J.; Rega, N.; Zheng, G.; Liang, W.; Hada, M.; Ehara, M.; Toyota, K.; Fukuda, R.; Hasegawa,  
558 J.; Ishida, M.; Nakajima, T.; Honda, Y.; Kitao, O.; Nakai, H.; Vreven, T.; Throssell, K.;

559 Montgomery Jr., J. A.; Peralta, J. E.; Ogliaro, F.; Bearpark, M. J.; Heyd, J. J.; Brothers, E. N.;  
560 Kudin, K. N.; Staroverov, V. N.; Keith, T. A.; Kobayashi, R.; Normand, J.; Raghavachari, K.;  
561 Rendell, A. P.; Burant, J. C.; Iyengar, S. S.; Tomasi, J.; Cossi, M.; Millam, J. M.; Klene, M.;  
562 Adamo, C.; Cammi, R.; Ochterski, J. W.; Martin, R. L.; Morokuma, K.; Farkas, O.;  
563 Foresman, J. B.; Fox, D. J. Gaussian 09 Rev. D.01, 2013.  
564 (64) Werner, H.-J.; Knowles, P. J.; Knizia, G.; Manby, F. R.; Schütz, M. Molpro: A  
565 General-Purpose Quantum Chemistry Program Package. *WIREs Computational Molecular*  
566 *Science* **2012**, 2 (2), 242–253. <https://doi.org/10.1002/wcms.82>.  
567 (65) Martin, J. M. L. Ab Initio Total Atomization Energies of Small Molecules — towards  
568 the Basis Set Limit. *Chemical Physics Letters* **1996**, 259 (5–6), 669–678.  
569 [https://doi.org/10.1016/0009-2614\(96\)00898-6](https://doi.org/10.1016/0009-2614(96)00898-6).  
570 (66) Feller, D.; Dixon, D. A. Extended Benchmark Studies of Coupled Cluster Theory  
571 through Triple Excitations. *The Journal of Chemical Physics* **2001**, 115 (8), 3484–3496.  
572 <https://doi.org/10.1063/1.1388045>.  
573